

Broadband angular color stability of dielectric thin film-coated pyramidal textured Si for photovoltaics

Cite as: J. Appl. Phys. 129, 173104 (2021); doi: 10.1063/5.0048102

Submitted: 19 February 2021 · Accepted: 18 April 2021 ·

Published Online: 7 May 2021



View Online



Export Citation



CrossMark

N. Roosloot,^{1,a,b)} V. Neder,^{2,c)} H. Haug,³ C. C. You,³ A. Polman,⁴ and E. S. Marstein¹

AFFILIATIONS

¹Department of Solar Power Systems, Institute for Energy Technology, NO-2027 Kjeller, Norway

²Institute of Physics, University of Amsterdam, Science Park 904, 1098 XH Amsterdam, The Netherlands

³Department of Solar Cell Technology, Institute for Energy Technology, NO-2027 Kjeller, Norway

⁴Center for Nanophotonics, AMOLF, Science Park 104, 1098 XG Amsterdam, The Netherlands

^{a)}**Author to whom correspondence should be addressed:** nathan.roosloot@ife.no

^{b)}**Also at:** Institute of Physics, University of Amsterdam, Science Park 904, 1098 XH Amsterdam, The Netherlands.

^{c)}**Also at:** Center for Nanophotonics, AMOLF, Science Park 104, 1098 XG Amsterdam, The Netherlands.

ABSTRACT

In this work we demonstrate the angular color stability of textured c-Si substrates colored by single layer thin film coatings of SiN_x . These coatings show higher angular color stability on substrates with a random upright pyramidal surface texture compared to identical coatings on planar silicon substrates. Angle dependent reflectance measurements, supported by a modeling framework, display that the reflectance peaks originating from thin film interference of coated textured substrates only shift about 15 nm with an increasing angle of incidence from 10° to 80° , while the reflectance peaks of planar substrates with identical coatings shift about 120 nm at these angles. More specifically, reflectance peaks of planar substrates shift to shorter wavelengths, leading to a blue shift of the color appearance. The stable peak position of the textured samples is explained by a 2D representation of their surface texture and the primarily double interference interaction on it. While it is well known that a wide range of colors can be realized exhibiting low optical losses with thin film coatings, angular color stability was often not taken into account. However, for building integrated photovoltaics applications, a high angular color stability is desired, underlining the importance of using these textures. In most installed c-Si photovoltaics, similar substrate surface textures and dielectric thin film layers are already used. Therefore, this work envisions a route to facilitate large scale production of colored solar cells on textured c-Si substrates, colored by thin film SiN_x layers, with minimized optical losses and improved angular color stability.

Published under an exclusive license by AIP Publishing. <https://doi.org/10.1063/5.0048102>

I. INTRODUCTION

Two key aspects of building-integrated photovoltaic (BIPV) elements are their aesthetics and power output. Ideally, BIPV elements are desired components of a building from an aesthetic point of view, while also producing as much power as possible. In the case of colored BIPV, these two aspects are often conflicting, as light in the visible range needs to be reflected to create color. Since this light would otherwise be transmitted to the active layers of the cell, coloring a BIPV product decreases its power output. It is thus an important challenge to create solar cells with a wide range of possible colors at minimized optical losses.

As both the PV and BIPV market are dominated by crystalline silicon (c-Si) technologies,¹ it is especially important to create inexpensive and efficient ways to color c-Si based solar cells. Most c-Si based colored BIPV products that are currently present on the market are based on printing techniques.¹ Although inexpensive and easily integrated into the PV manufacturing process, these techniques come with high optical losses.² A more efficient way to color c-Si cells is via deposition of thin film coatings on top of the silicon substrate. Such coatings have spectrally selective reflectance spectra due to interference. By varying the thickness and refractive index of this film, a wide variety of colors with high transmission

into the active layers of the cell can be achieved.^{3–8} In particular, films made of silicon nitride (a-SiN_x:H, also called SiN_x), deposited by plasma-enhanced chemical vapor deposition (PECVD), allow for immediate large scale production of colored solar cells, as they are already deposited onto c-Si solar cells in standard manufacturing as the anti-reflection coating (ARC). This is a major benefit of this technique over a variety of other novel solar cell coloring techniques based on, for example, scatterers,^{9,10} plasmonic structures,¹¹ and other nanostructures,^{12–14} which have also shown to color solar cells with little optical losses but are not yet ready to be implemented on a factory scale. There exists extensive research on coloring with thin films, but little focus has been dedicated to the angular color stability of these coatings, which is important to the BIPV market. When using this coloring method on planar substrates, the color appearance of the film is strongly influenced by the angle of incidence of incoming light, as this determines the effective thickness of the thin film. The great majority of installed c-Si PV is based on substrates that are not planar, but have some surface texture. In the case of monocrystalline silicon, a random upright pyramid texture, created by wet alkaline etching, is most commonly used.^{15–18} This texture reduces reflectance and increases light trapping, and thus contributes to an increase in the current output of the solar cell^{15,19–21} and is also cheaper to realize than a perfectly planar substrate surface. In this paper, it is shown that such substrates colored with single layer thin film coatings possess better angular color stability than planar substrates coated with identical coatings. Experimental measurements of angle dependent reflectance of the samples are supported by modeled spectra, and the angular stability of the textured surfaces is explained using a 2D representation of the surface texture. In total, four different thin film coatings, each with a different color, were deposited and compared. As the conclusions are the same for all four films, only the full analysis of one of these, a film with a green color appearance, called sample G1, will be shown here. More information on the other samples can be found in the [supplementary material](#).

II. THEORETICAL METHODS

Because reflected light from a single thin film on top of a substrate consists of two beams, interference of light occurs. By changing thickness or index of the thin film, the wavelengths at which this happens can be tuned and the color appearance of the film can be modified. For constructive interference to occur at wavelength λ , the optical path difference between the two reflected beams should be equal to $m_1 \cdot \lambda$, with $m_1 \in \mathbb{N}$. Therefore, one can easily derive that for a planar thin film of thickness d , constructive interference occurs at wavelengths

$$\lambda_{max} = \frac{2n_1 d}{m_1} \sqrt{1 - \left(\frac{n_0}{n_1} \sin \theta \right)^2}, \quad (1)$$

where n_0 and n_1 are the refractive indices of the surrounding medium, in this work air, and the thin film layer, respectively, and θ is the angle of incidence on the thin film. To determine at which wavelengths destructive interference occurs, one can simply substitute m_1 for $(m_2 + \frac{1}{2})$ with $m_2 \in \mathbb{N}_0$. From this follows that as θ

increases, the positions of the reflectance minima and maxima shift toward bluer wavelengths, impacting the color appearance of the thin film. For substrates with a random upright pyramid texture, reflected light is made up of beams following a large amount of discrete paths, which each have one or multiple interactions with the substrate under different angles of incidence.¹⁵ A change in the angle of incidence does therefore not necessarily result in a shift in the wavelengths of minimum and maximum reflectance.

In this work, the measured reflectance spectra of planar thin films are compared to modeled reflectance spectra, based on the model created by Haug *et al.*²² which uses the transfer matrix method. As the reflectance of textured substrates cannot be modeled in this way, the online ray tracing tool OPAL 2^{23,24} was used to model the reflectance spectra of the textured substrates. It is not expected that the reflectance modeled by ray tracing will be exactly the same as what is measured, as such models often assume an ideal upright pyramid surface texture, where all pyramids have the same base angle. It has been observed, however, that the pyramid base angles often have a distribution of values below the theoretical angle of 54.7° as a result of non-ideal etching.^{16–18,25} Furthermore, it has been shown that the surface texture can have features of hillocks with an orthogonal base, rather than of pyramids, making ray tracing approximations less exact.²⁵ Finally, scattering and/or diffraction effects at pyramids with a size around the wavelength of light, or at the edges and tips of larger pyramids are not taken into account in most traditional ray tracing.^{26,27} Despite these shortcomings, modeled reflectance of textured substrates with ray tracing might still give insight into the expected behavior of ideal pyramid textures.

In addition to the modeling work, the color of all samples is calculated and expressed in both RGB coordinates and the chromaticity at the measured angles of incidence using the CIE 1931 2 degrees standard observer.²⁸

III. EXPERIMENTAL METHODS

As planar substrates, p-type (100) double side polished monocrystalline silicon wafers grown by the Czochralski method were used. The wafers have a thickness of $275 \pm 20 \mu\text{m}$ and a resistivity of $1–10 \Omega \text{ cm}$ and are cut into $30 \times 30 \text{ mm}$ pieces. To create substrates with a random upright pyramid texture on both sides of the wafer, the polished wafers were etched for 30 min in a KOH based solution. This solution was created by mixing 11.5 l of water with 517 ml of a 48% KOH solution, which was consecutively heated up to 80 °C. Once this temperature was reached, 180 ml of a proprietary buffering agent and 18 ml of a texturizer additive were added. A nitrogen bubble flow was present in the solution during the entire etching process to promote chemical mixing. After etching, wafers were consecutively rinsed in baths of de-ionized (DI) water, hydrochloric acid solution and DI water, and dried with a nitrogen gas flow. The textured samples shown in this work have a quarter circle shape with a radius of 30 mm. Scanning electron microscopy (SEM) measurements were carried out to ensure that no planar fractions were present on the surface. An example of this is shown in Fig. SM1 of the [supplementary material](#). To remove the native oxide layer on the samples before depositions, all samples were put in a 5% hydrogen fluoride (HF) bath for 2 min and subsequently rinsed with DI water and then dried with a nitrogen gas flow.

All thin films were deposited with an Oxford instruments plasma lab system 133 under a radio frequency (RF) power of 40 W, a reaction chamber pressure of 800 mTorr, and a temperature of 350 °C. SiN_x films were created using SiH₄ and NH₃ gas flows. A N₂ background flow of 980 SCCM was used for all depositions. The other gas flows as well as the deposition time varied per sample, depending on the required refractive index and thin film thickness.

The thickness, as well as its accuracy, and the optical data of the thin films on planar substrates were determined by ellipsometry, using a variable angle spectroscopic ellipsometer (VASE) from J. A. Woollam. All samples were characterized from 300 to 1000 nm with 5 nm intervals using the same measurement parameters, which can be found in the [supplementary material](#).

Ellipsometric data were fitted using the WVASE32 software from Woollam, using Cauchy or Tauc-Lorentz oscillators, depending on whether the thin films were light absorbant below 600 nm or not. The resulting optical data of the green sample are shown in Fig. SM2 of the [supplementary material](#).

The angle dependent reflectance was measured with an integrating sphere setup. A Spectral Products QTH 30 W ASB-W-030 high stability tungsten-halogen light in combination with an Oriel Cornerstone 260 monochromator from Newport was used as a light source. To modulate the intensity of the light beam and improve the signal-to-noise ratio, the beam was sent through a chopper and lock-in amplifier. The beam was then focused by a series of lenses and depolarized by a depolarizer before entering a 6 in. RTC-060-SF integrating sphere from Labsphere, in which samples were placed inside via a clip-style center mount sample holder. Reflected light was detected with a S1336-5BQ silicon detector from Hamamatsu. All measurements were performed between 350 and 1000 nm, with 5 nm intervals. The reflectance was therefore modeled with the same wavelength domain and intervals. It was observed that from 950 nm, measured reflectance increased for all samples as the substrates became partially transparent. All samples were measured from the

zenith angle $\theta = 10^\circ$ to 80° with 10° intervals and results are shown in Figs. 1 and 2 and discussed in the next section.

The thickness of the thin films on the textured substrates could not be determined with ellipsometry, as the reflected light missed the detector due to the surface texture. An estimation of the thickness was therefore made by measuring the reflectance of the samples at the mentioned angles and using Eq. (1) to calculate the thickness. Although this equation is only valid for planar films, it has been demonstrated²⁹ that this is also a good approximation to determine thin film thickness on textured substrates, as the reflectance minima of textured and polished substrates with identical thin films are typically not far off. Transmission electron microscopy (TEM) measurements on other samples were carried and confirmed that this method determines the thickness of the thin film accurately within 5 nm. These measurements were carried out along multiple cross sections of the samples to confirm uniform thin film layer thickness.

From the measured reflectance spectra, the colors and chromaticities of the samples were calculated as shown in Fig. 3 and discussed below. This calculation is based on the overlap of the reflectance spectra and the color matching functions of the RGB and XYZ color spaces, respectively. This allows the color belonging to any reflectance spectrum to be expressed in the tristimulus values of the respective color spaces, which are used to quantify color and chromaticity.^{28,30}

IV. RESULTS AND DISCUSSION

As can be seen in Table I, the thin film thickness of the samples is almost identical for the planar and textured substrates. Since the thin films are deposited under the same deposition parameters, it is assumed that the optical data are equal.

In Fig. 1, one can see the measured and modeled angle dependent reflectance from both the polished and textured samples for incoming angles from $\theta = 10^\circ$ to $\theta = 80^\circ$. Figure 1(a) shows that

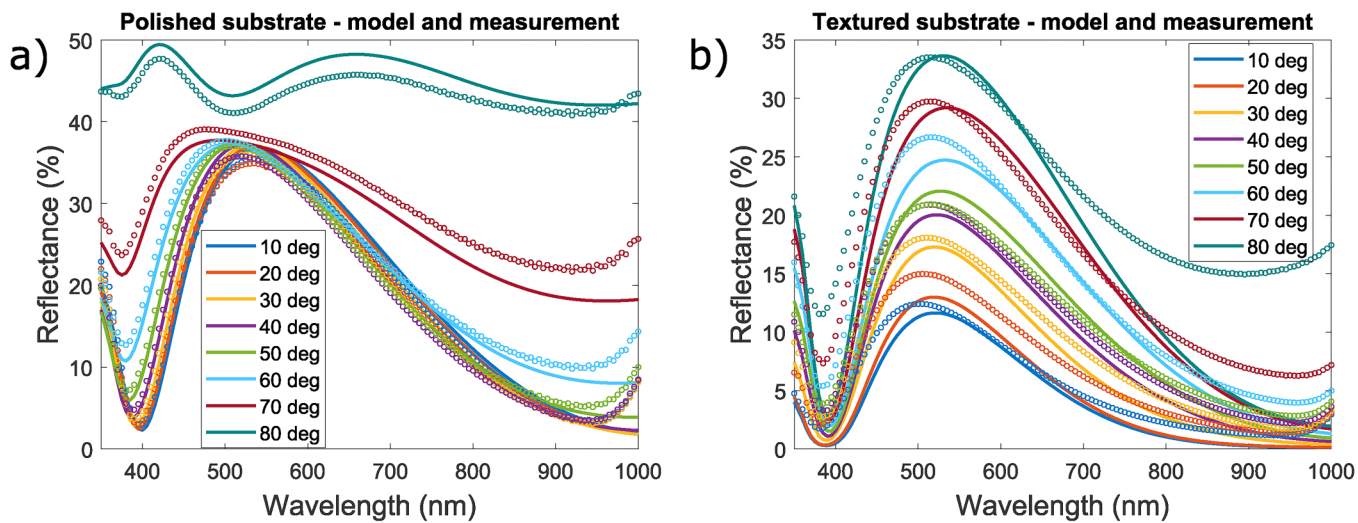


FIG. 1. Measured (symbols) and modeled (lines) angle dependent reflectance of sample G1 on polished silicon (a) and on textured silicon (b).

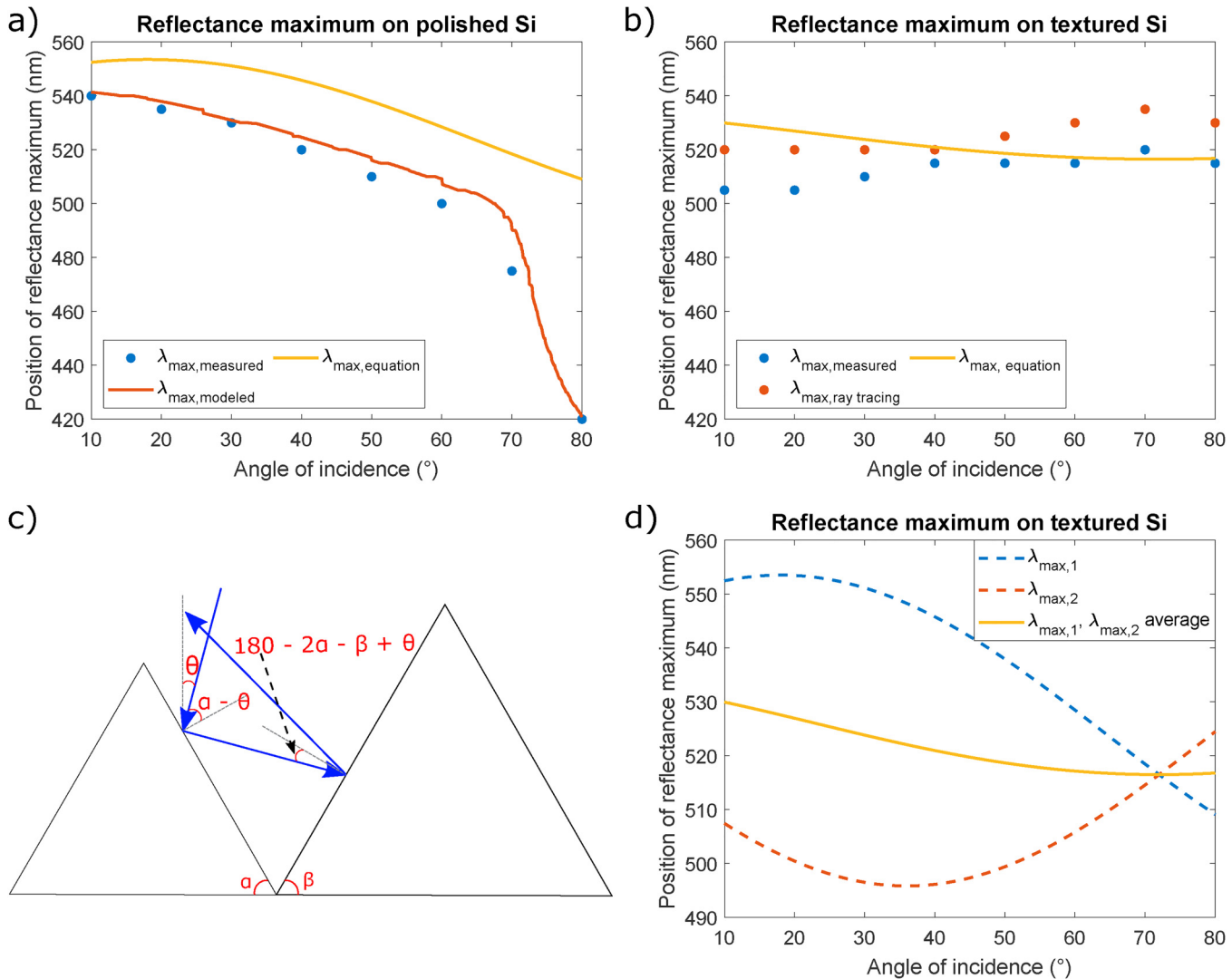


FIG. 2. (a) Position of reflectance maxima of G1 on polished silicon as measured (blue dots), modeled (red dots) and calculated (yellow solid line) using Eq. (1), (b) Position of reflectance maxima of G1 on textured silicon as measured (blue dots), modeled (red solid line) and calculated (yellow solid line), (c) path of reflected light under incoming angle θ on a textured substrate and (d) calculated reflectance maxima of G1 on textured silicon from Eq. (2) (blue dashed line), Eq. (3) (red dashed line), and the average of both equations (yellow solid line).

the modeled and measured reflectance of the polished sample are generally in good agreement, with some exceptions for higher angles of incidence. The positions of the reflectance minima and maxima shift around 40 nm to shorter wavelengths when the incoming angle increases from 10° to 60° , and an additional 80 nm when the incoming angle increases from 60° to 80° .

The measured and modeled reflectance of the textured sample are shown in Fig. 1(b), and the positions of the reflectance minima and maxima are in reasonable agreement. However, there are differences in the intensities of the modeled and measured reflectance spectra, with the modeled reflectance generally being higher than the measured reflectance outside the reflectance maxima. These

discrepancies can be caused by the shortcomings of the ray tracing model, which have been discussed before. Most importantly, one can see that in both cases the positions of the reflectance minima and maxima are stable under an increase in the angle of incidence, with a total shift of only about 15 nm under an increase from 10° to 80° .

One can also see that in general the reflectance of the textured sample is much lower than that of the polished one. As a result, identical thin films will have a darker color appearance on textured substrates than on polished ones, which might be a disadvantage when trying to reach bright colors. Figure 1 also shows that the reflectance of the textured sample increases much more with an increase in the angle of incidence than that of the polished sample.

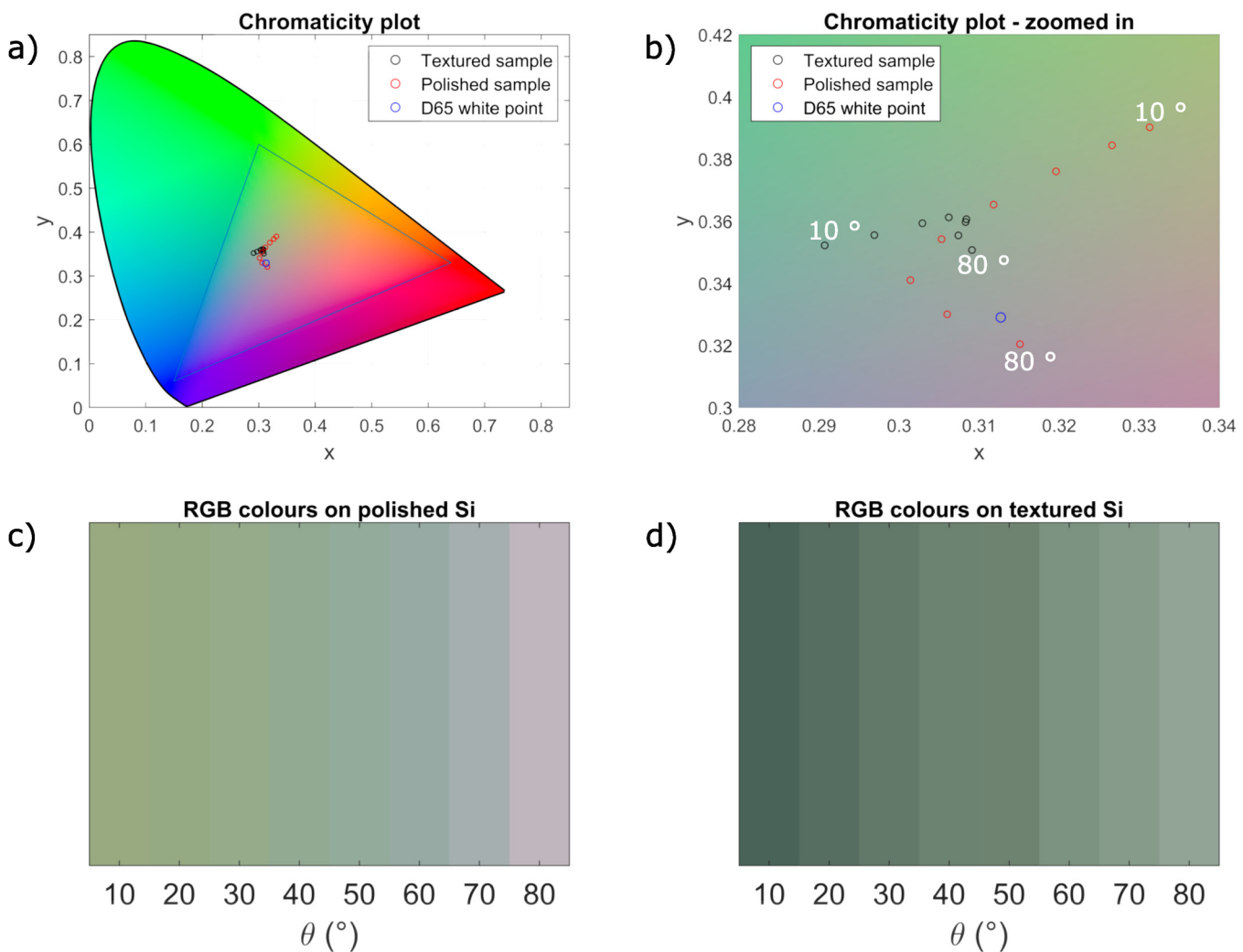


FIG. 3. Chromaticity diagram of the polished and textured samples at angles of incidence 10° to 80° (a), with additional zoom around the relevant area (b), together with color patches of the polished (c) and textured (d) samples at angles of incidence 10° to 80° .

This can be explained by the fact that the double bounce effect that usually decreases reflectance from textured samples is not that effective anymore for large angles of incidence.^{31,32}

Figures 2(a) and 2(b) show the measured (blue dots), modeled (red solid line and dots), and calculated (yellow line) positions of the reflectance maxima with changing incoming angles for the planar

and textured samples. The measured positions were extracted from the measurements shown in Fig. 1. For the planar sample, the peak positions were modeled with a precision of 0.1 nm at angles of incidence 10° to 80° at 0.1° intervals using the model based on the transfer matrix method, and for the textured sample the peaks were extracted from the modeled data plotted in Fig. 1(b), which were determined by the OPAL model that was described above. Figures 2(a) and 2(b) show that the modeled and measured reflectance maxima are in good agreement for both substrates.

In Fig. 2(a), the positions of the reflectance maxima are also calculated using Eq. (1). All three curves in Fig. 2(a) show the expected blueshift of the reflectance maxima. However, at high angles of incidence, the positions of the reflectance maxima as calculated by Eq. (1) deviate from the modeled and measured positions. This is due to the fact that at these angles, internal reflectance becomes

TABLE I. Thickness of thin film G1 on polished and textured substrate, determined by ellipsometry and angle dependent reflectance measurements, respectively.

Sample name	Substrate	Film thickness (nm)
Green (G1)	Polished	125.3 ± 0.1
	Textured	123.0 ± 5.0

significant. As a result, the reflectance spectra largely consist of direct reflectance from the thin film, while the effects of interference decrease. This is taken into account by the optical model, which calculates the full reflectance of the sample, but not by Eq. (1).

In Fig. 2(b), one can see that both the measured and the modeled reflectance maxima of the textured sample are much more stable against changes in the angle of incidence than those of the polished sample. This can be explained by considering the way in which light reflection depends on the angle of incidence on the textured substrate surface. Under normal incidence, about 68% of light incident on the textured substrate surface is reflected along the same path,¹⁵ which is described in Fig. 2(c) for an angle of incidence θ . By treating the two pyramids independently, we can describe the reflectance maximum that is caused by each pyramid using Eq. (1),

$$\lambda_{max,1} = \frac{2n_1 d}{m_1} \sqrt{1 - \left(\frac{n_0}{n_1}\right)^2 \sin^2(\alpha - \theta)}, \quad (2)$$

$$\lambda_{max,2} = \frac{2n_1 d}{m_1} \sqrt{1 - \left(\frac{n_0}{n_1}\right)^2 \sin^2(180 - 2\alpha - \beta + \theta)}. \quad (3)$$

Here, $\lambda_{max,1}$ and $\lambda_{max,2}$ stand for the reflectance maxima caused by pyramids 1 and 2, as indicated in Fig. 2(c). As both pyramids are coated with the same thin film, n_0 , n_1 , m_1 , and d are the same for both equations. Since α and β are constant, we can see that under a change in the angle of incidence θ , the two reflectance maxima shift in the opposite direction for most values of α and β . Since we measure only one reflectance minimum and not two for these coated substrates, it is likely that the measured reflectance maximum is the average of the two maxima $\lambda_{max,1}$ and $\lambda_{max,2}$. Under the assumptions that $\alpha = \beta = 54.7^\circ$, and $n_1 = 2.25$ at all wavelengths, the positions of the two maxima $\lambda_{max,1}$ (blue dashed line) and $\lambda_{max,2}$ (red dashed line) and their average (yellow line) at different angles of incidence are shown in Fig. 2(d). In Fig. SM2a of the [supplementary material](#), one can see that at wavelengths from 500 to 550 nm, which is where the reflectance maxima occur

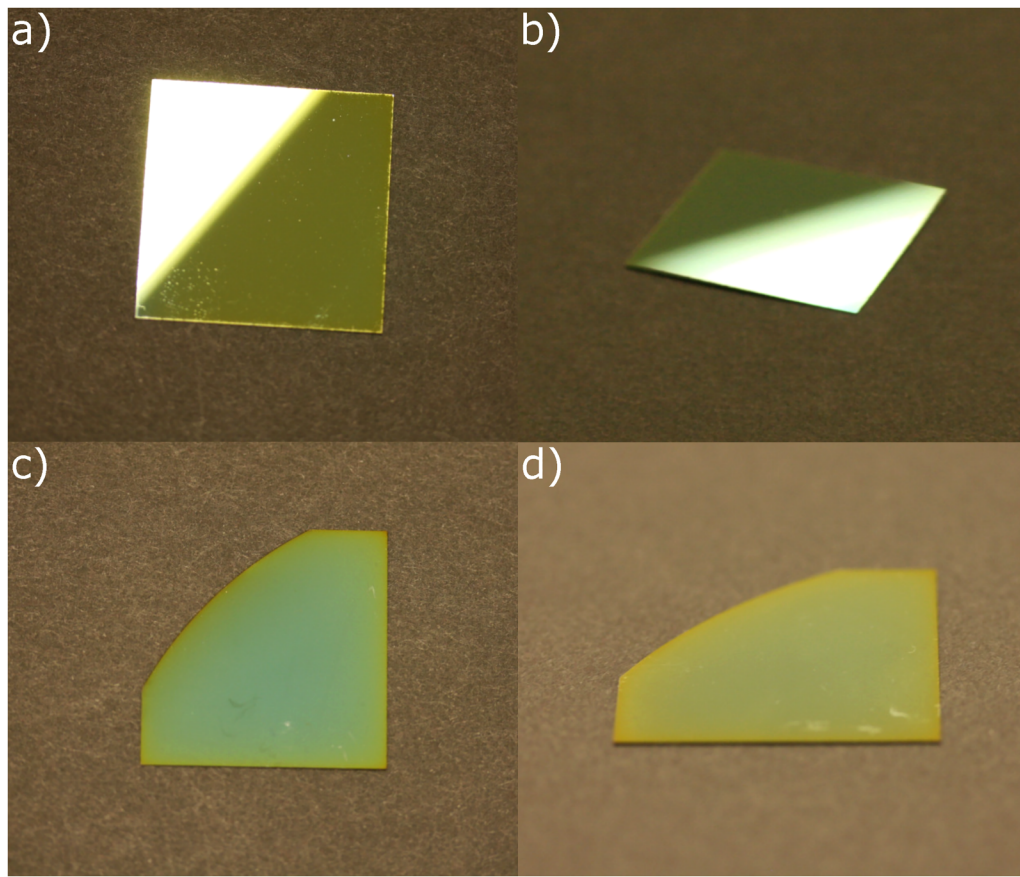


FIG. 4. Photographs of the polished (a) and (b) and textured (c) and (d) sample, taken under office lighting at 15° [(a) and (c)] and 60° [(b) and (d)]. The same black paper is used as background for all samples, but seems to have a different color in some photographs due to variations in the camera exposure time. The polished substrates are 30×30 mm, and the textured ones have a radius of 30 mm.

at most angles of incidence, $n = 2.23 - 2.26$. The assumption that $n = 2.25$ at all wavelengths thus does not impact the position of the calculated reflectance maximum much.

The average of $\lambda_{max,1}$ and $\lambda_{max,2}$ is also plotted with the measured reflectance maxima of the textured films in Fig. 2(b) (yellow line). Indeed, Fig. 2(b) shows that the average of $\lambda_{max,1}$ and $\lambda_{max,2}$ is in fairly good agreement with the measured reflectance maxima of the textured sample.

The effect of the (in)stability of the reflectance extrema can clearly be seen when looking at the colors of the samples at different angles of incidence, as shown in Fig. 3. Figure 3(c) demonstrates that the colors of the polished sample become bluer as the angle of incidence increases. On the other hand, the color of the textured sample, which is as expected much darker than that of the polished sample, remains green under a change in the angle of incidence, as shown in Fig. 3(d). The color of this sample does become brighter with an increase in the angle of incidence as the magnitude of the reflectance increases, with Y increasing from 0.10 at 10° to 0.32 at 80° . This is caused by the fact that at higher angles of incidence, more light will take paths which are only incident on the textured substrate surface once instead of twice or more.

The difference in color stability between the respective samples is especially apparent when one looks at their chromaticities, which are shown in Figs. 3(a) and 3(b). While the chromaticity of the textured sample remains relatively stable, that of the polished sample changes to blue chromaticities more drastically, before changing to a more purple region at high angles of incidence, as the reflectance spectra completely change due to a decrease in the effect of interference. In the supplementary material, the colors and chromaticities of the three samples with different colors are shown. There, too, samples on textured substrates show a stronger color stability than those on polished ones.

This is also seen when looking at photographs of the samples taken under varying angles of incidence, as shown in Fig. 4. All photographs are taken under office lighting, which influences the observed color of the samples. This is most clearly visible in Figs. 4(a) and 4(b): the light patch on the samples is caused by direct illumination of the office lamps, while the darker regions show the color that best agrees with what is observed with the naked eye. Furthermore, the photographs show the advantage of creating matte colors with the textured samples over shiny colors on the polished ones. This is beneficial for BIPV applications as glare effects are avoided. To image the observed color of the samples as accurately as possible, different camera exposure times were used, which affect the color of the background. The photographs clearly demonstrate the color change of the samples. Figures 4(a) and 4(b) show that the color of the polished sample changes from a yellow-green color at 15° to a green-blue color at 60° . Figures 4(c) and 4(d) show that the textured sample, on the other hand, remains green at both angles of incidence, but with different brightness. The samples show slight color inhomogeneities around the edges, which are caused by thin film thickness variations from the PECVD depositions.

V. CONCLUSION

In this work, it has been shown that dielectric thin film-coated silicon substrates with a pyramidal surface texture have a much

stronger angular color stability than planar substrates with identical coatings. This has been shown by angle resolved reflectance measurements of fabricated planar and textured colored c-Si substrates. It has been found that the color stability can be explained by the primarily averaged double interference on the pyramids of the textured substrates. This is a major benefit for building integrated photovoltaic applications, as stable colors are often desired for aesthetic integration into the built environment. Considering that the textured substrates in this work are widely used in commercial c-Si PV, this thin film coloring technique on textured substrates might be ready to be applied on a large scale.

SUPPLEMENTARY MATERIAL

See the [supplementary material](#) for an SEM image of the textured substrate surface texture, as well as the ellipsometric measurement parameters, the refractive index of the sample, and thin film thickness and color plots of three additional samples.

ACKNOWLEDGMENTS

Erik Stensrud Marstein and Halvard Haug acknowledge funding from the research center FME SUSOLTECH (NFR Project No. 257639), which is co-financed by the center partners and the Research Council of Norway. The AMOLF part of this work is part of the research program of the Dutch National Science Counsel (NWO).

DATA AVAILABILITY

The data that support the findings of this study are available from the corresponding author upon reasonable request.

REFERENCES

- ¹G. Eder, G. Peharz, R. Trattning, P. Bonomo, E. Saretta, F. Frontini, C. S. Polo Lopez, H. Rose Wilson, J. Eisenlohr, N. Martín Chivelet, S. Karlsson, N. Jakica, and A. Zanelli, "COLOURED BIPV Market, research and development IEA PVPS Task 15," Report IEA-PVPS T15-07 (2019).
- ²C. Kutter, B. Bläsi, H. Rose Wilson, T. Kroyer, M. Mittag, O. Höhn, and M. Heinrich, "Decorated building-integrated photovoltaic modules: Power loss, color appearance and cost analysis," in 35th European PV Solar Energy Conference and Exhibition, 2018, pp. 1488–1492.
- ³A. Schüller, J. Boudaden, P. Oelhafen, E. De Chambrier, C. Roecker, and J.-L. Scartezzini, "Thin film multilayer design types for colored glazed thermal solar collectors," *Sol. Energy Mater. Sol. Cells* **89**, 219–231 (2005).
- ⁴J. Selj, T. Mongstad, R. Søndenå, and E. Marstein, "Reduction of optical losses in colored solar cells with multilayer antireflection coatings," *Sol. Energy Mater. Sol. Cells* **95**, 2576–2582 (2011).
- ⁵M. Li, L. Zeng, Y. Chen, L. Zhuang, X. Wang, and H. Shen, "Realization of colored multicrystalline silicon solar cells with SiO₂/SiNx:H double layer antireflection coatings," *Int. J. Photoenergy* **2013**, 352473.
- ⁶L. Zeng, M. Li, Y. Chen, and H. Shen, "A simplified method to modulate colors on industrial multicrystalline silicon solar cells with reduced current losses," *Sol. Energy* **103**, 343–349 (2014).
- ⁷M. Amara, F. Mandorlo, R. Couderc, F. Gerenton, and M. Lemiti, "Temperature and color management of silicon solar cells for building integrated photovoltaic," *EPJ Photovoltaics* **9**, 1 (2018).
- ⁸B. Bläsi, T. Kroyer, O. Höhn, M. Wiese, C. Ferrara, U. Eitner, and T. E. Kuhn, "Morpho butterfly inspired coloured bipv modules," in 33rd European PV Solar Energy Conference and Exhibition, 2017.

- ⁹V. Neder, S. L. Luxembourg, and A. Polman, "Efficient colored silicon solar modules using integrated resonant dielectric nanoscatterers," *Appl. Phys. Lett.* **111**, 073902 (2017).
- ¹⁰V. Neder, S. L. Luxembourg, and A. Polman, "Colored solar modules using integrated pixelated resonant dielectric nanoscatterer arrays," in 33rd European Photovoltaic Solar Energy Conference and Exhibition, 2017, pp. 34–37.
- ¹¹G. Peharz, B. Grosschädl, C. Prietl, W. Waldhauser, and F. Wenzl, "Tuning the colors of C-Si solar cells by exploiting plasmonic effects," in *Next Generation Technologies for Solar Energy Conversion VII* (International Society for Optics and Photonics, 2016), Vol. 9937, p. 99370P.
- ¹²S. Chhajed, M. F. Schubert, J. K. Kim, and E. F. Schubert, "Nanostructured multilayer graded-index antireflection coating for Si solar cells with broadband and omnidirectional characteristics," *Appl. Phys. Lett.* **93**, 251108 (2008).
- ¹³M.-L. Kuo, D. J. Poxson, Y. S. Kim, F. W. Mont, J. K. Kim, E. F. Schubert, and S.-Y. Lin, "Realization of a near-perfect antireflection coating for silicon solar energy utilization," *Opt. Lett.* **33**, 2527–2529 (2008).
- ¹⁴L. Cao, P. Fan, E. S. Barnard, A. M. Brown, and M. L. Brongersma, "Tuning the color of silicon nanostructures," *Nano Lett.* **10**, 2649–2654 (2010).
- ¹⁵S. C. Baker-Finch and K. R. McIntosh, "Reflection of normally incident light from silicon solar cells with pyramidal texture," *Prog. Photovoltaics Res. Appl.* **19**, 406–416 (2011).
- ¹⁶E. Fornies, C. Zaldo, and J. Albella, "Control of random texture of monocrystalline silicon cells by angle-resolved optical reflectance," *Sol. Energy Mater. Sol. Cells* **87**, 583–593 (2005).
- ¹⁷A. A. Fashina, M. G. Z. Kana, and W. O. Soboyejo, "Optical reflectance of alkali-textured silicon wafers with pyramidal facets: 2D analytical model," *J. Mater. Res.* **30**, 904–913 (2015).
- ¹⁸S. Manzoor, M. Filipič, A. Onno, M. Topič, and Z. C. Holman, "Visualizing light trapping within textured silicon solar cells," *J. Appl. Phys.* **127**, 063104 (2020).
- ¹⁹A. M. Al-Husseini and B. Lahlouh, "Influence of pyramid size on reflectivity of silicon surfaces textured using an alkaline etchant," *Bull. Mater. Sci.* **42**, 152 (2019).
- ²⁰H. Park, S. Kwon, J. S. Lee, H. J. Lim, S. Yoon, and D. Kim, "Improvement on surface texturing of single crystalline silicon for solar cells by saw-damage etching using an acidic solution," *Sol. Energy Mater. Sol. Cells* **93**, 1773–1778 (2009).
- ²¹Y. Jiang, X. Zhang, F. Wang, and Y. Zhao, "Optimization of a silicon wafer texturing process by modifying the texturing temperature for heterojunction solar cell applications," *RSC Adv.* **5**, 69629–69635 (2015).
- ²²H. Haug, J. Selj, Ø. Nordseth, and E. Marstein, "Optimization of a-SiO_x/a-SiNx double layer antireflection coatings for silicon solar cells," in 27th European Photovoltaic Solar Energy Conference and Exhibition, 2012, pp. 1376–1378.
- ²³OPAL 2, available at <https://www2.pvlighthouse.com.au/calculators/OPAL%202/OPAL%202.aspx> (accessed July 15, 2020).
- ²⁴K. R. McIntosh and S. C. Baker-Finch, "Opal 2: Rapid optical simulation of silicon solar cells," in 2012 38th IEEE Photovoltaic Specialists Conference (IEEE, 2012), pp. 000265–000271.
- ²⁵S. C. Baker-Finch and K. R. McIntosh, "Reflection distributions of textured monocrystalline silicon: Implications for silicon solar cells," *Prog. Photovoltaics Res. Appl.* **21**, 960–971 (2013).
- ²⁶O. Höhn, N. Tucher, and B. Bläsi, "Theoretical study of pyramid sizes and scattering effects in silicon photovoltaic module stacks," *Opt. Express* **26**, A320–A330 (2018).
- ²⁷O. Höhn, N. Tucher, A. Richter, M. Hermle, and B. Bläsi, "Light scattering at random pyramid textures: Effects beyond geometric optics," *AIP Conf. Proc.* **1999**, 030002 (2018).
- ²⁸T. Smith and J. Guild, "The cie colorimetric standards and their use," *Trans. Opt. Soc.* **33**, 73 (1931).
- ²⁹A. Krieg, J. Greulich, M. Tondorf, and S. Rein, "Anti-reflection-coating thickness measurements on textured silicon surfaces: Evaluation and accuracy of different measurement techniques," in Proceedings of the 28th European Photovoltaic Solar Energy Conference and Exhibition, 2013, pp. 1820–1824.
- ³⁰I. E. Commission, "IEC 61966-2-1:1999," Multimedia Systems and Equipment—Colour Measurements and Management—Part2-1: Colour Management - Default RGB Colour Space - sRGB (IEC, 1999).
- ³¹A. Parretta, A. Sarno, P. Tortora, H. Yakubu, P. Maddalena, J. Zhao, and A. Wang, "Angle-dependent reflectance measurements on photovoltaic materials and solar cells," *Opt. Commun.* **172**, 139–151 (1999).
- ³²V. Magnin, J. Harari, M. Halbwax, S. Bastide, D. Cherfi, and J.-P. Vilcot, "Angle-dependent ray tracing simulations of reflections on pyramidal textures for silicon solar cells," *Sol. Energy* **110**, 378–385 (2014).